Dissolution Kinetics of Polymer Powders

Alan Parker
Firmenich S. A., CH-1211 Geneva 8, Switzerland

Florence Vigouroux
SKW Biosystems, 50500 Carentan, France

Wayne F. Reed
Physics Dept., Tulane University, New Orleans, LA 70118

The dissolution kinetics of polymer powders as isolated grains or in beds were studied theoretically and experimentally. A simple model developed for the dissolution of a dispersion of isolated grains with an arbitrary size distribution was confirmed experimentally using polysaccharides in water. Based on experimental data for the dissolution of lump-forming powder beds, modeled using a bimodal population of grains and lumps, a robust technique was developed for analyzing experimental data, which is independent of the details of lump formation. A qualitative picture of lump formation is described, based on the idea that during the initial hydration of a powder bed a ''pore blocking'' condition quickly develops due to the formation of a gel layer around the dry grains. Once formed, lumps dissolved the same way and with the same kinetic description, as individual, dispersed grains.

Introduction

Water-soluble polymers such as xanthan and pectin are typically dried and milled into powders (consisting of individual grains) after they are produced. Before use, the powders have to be dissolved in aqueous solution. The dissolution time is of critical importance in industrial and consumer applications, and is one of the factors that defines product quality. A further feature of dissolution is the phenomenon of lump formation, in which many grains adhere together and considerably slow the dissolution process. The tendency to form lumps is usually considered to be a measure of the ''dispersibility'' of the polymer powder, in contrast to the dissolution of individual grains.

Polymer grain dissolution is much more complicated than that of low molecular weight solids (Buckley and Berger, 1962; Tu and Ouano, 1977; Herman and Edwards, 1990; Peppas et al., 1994). The dissolution process can be considered as a heterogeneous reaction, involving three steps: Step 1. Entry of water through the grain surface to form a swollen gel layer; Step 2. Release of polymer from the gel layer; Step 3. Transfer of the released polymer chains into the bulk solution. Below, we demonstrate that Step 2 is the rate-controlling step.

Brochard and de Gennes (1983) briefly discussed the effects of swelling and reptation on the optimum particle size for dissolution of concentrated polymer droplets. More recently, Devotta et al. (1994a,b) and Ranade and Mashelkar (1995) have developed, and verified experimentally, a sophisticated model for the dissolution kinetics of a polymer particle in a stirred solution. Brochard and de Gennes (1983) reached the conclusion that when dissolution of a semidilute drop of polymer solution is rate limited by reptation, then the dissolution time will be independent of the drop size. Devotta et al. (1994b) experimentally found a dry polymer grain size, below which the dissolution time was size independent. In this work, however, we are always in the regime controlled by Step 2, where dissolution time depends on particle size, which is the usual case in industrial practice.

The gel layer that forms immediately after polymer/solvent contact is highly viscous and extremely sticky, so its presence can lead to problems of lump formation when powder beds are tipped into solvent. Lump formation has a great influ-

Correspondence concerning this article should be addressed to W. F. Reed.

ence on the dissolution kinetics and also causes experimental difficulties for measuring dissolution rates. Despite its technological importance, we have not found any previous studies of the formation of lumps during polymer dissolution, either experimental or theoretical.

For a given polymer with a unique chemical composition and distribution of molecular masses, the final, fully dissolved product in a given solvent is always identical, even though dissolution times can vary widely, depending on the nature of the dry material and the conditions under which the product is dissolved (agitation, temperature, ionic strength, use of dispersing agents, etc.) In addition to such polymeric properties as mass, charge, persistence length, and interparticle forces, the thermodynamic path followed to produce the dry polymeric powder, which confers density and internal grain structure, are of critical importance in determining dissolution time.

Experienced powder users have formulated a number of useful heuristic rules to avoid the problem of lump formation: (1) large grains are less prone to lump formation than small ones; as a corollary, the presence of a small fraction of small grains (''fines'') can greatly degrade the dispersibility; (2) all factors that increase the dissolution rate also increase lump formation, such as heating; (3) lump formation can be prevented by thoroughly mixing the polymer powder with an excess of rapidly dissolving nonpolymeric diluant. This is termed ''dispersing conditions.'' Sugar is often used in the food industry. Furthermore, the diluant is most effective when it has a particle size similar to that of the polymer powder. The putative dispersion mechanism is that the polymer grains are sufficiently far from each other that solvent can penetrate the powder bed via the interstices left by the dissolved sugar, before the slowly dissolving polymer grains can stick together into a lump. Another dispersing method is to add the polymer powder slowly into the stirred solvent so that the grains are widely separated before they hydrate. When no such dispersing method is used, dissolution is said to take place under ''nondispersing conditions.''

This work concentrates on the influence of grain size, polydispersity, and dispersants on the dissolution kinetics and dispersibility of pectin and other polysaccharides. A simple integral transform for dissolution of polydisperse particles is presented and useful limits of this model are found and related to parameters very simply obtained from dissolution experiments, such as the time-dependent viscosity technique of Kravtchenko et al. (1999). The technique is then applied to various polysaccharides, from which the kinetic parameters and main trends are found and discussed.

An extension of the dissolution monitoring to include real-time measurements of light scattering and refractive index, in addition to viscosity, has recently been presented (Michel and Reed, 2000).

Materials and Methods

The polymer powders used were pectin, xanthan, carrageenan, and guar powders from SKW Biosystems. The powders were prepared, following usual industrial practice, by precipitating hot aqueous solution in isopropanol, then drying at 100°C. Finally, the material was milled to produce the final powder. The dry powder was fractionated by size using a Retsch vibrating sieve. The fractions were sized using a Malvern Mastersizer for low-angle light scattering. Pectin has a low persistence length and the sample used contains about 25% charged monomers. Guar has a low persistence length and has no charged monomers. Xanthan has a very high persistence length and contains 20% charged monomers.

The method used to determine the dissolution kinetics has been previously described (Kravtchenko et al., 1999). The method is described in detail, as the exact geometry of the powder addition process has a large impact on the result. Dissolution occurs in a crystallizing dish 65 mm high by 110 mm in diameter. The dish contains 300 g of water that is stirred using a four-bladed paddle mixer turned at 240 rpm. The blades are vertical plates 32 mm long by 14 mm deep. At time zero, a fixed amount of powder was automatically tipped from a PTFE-coated pot placed 5 cm above the surface of the water. For measurements under nondispersing conditions, 1 g of powder was used. For dispersing conditions, the powder was carefully mixed with ground sugar of roughly the same grain size. Eighteen grams of sugar and 1 g of powder gave immediate dispersion, with only a few transient lumps lasting a few seconds in the worst case. The impeller was connected to a torque transducer that provided a continuous measurement of the solution viscosity. The overlap concentration for the largest molecular-weight pectin was about 7 mg/mL, so that the concentrations in all experiments were below the overlap concentration c^*. Hence, the solvent-subtracted viscosity was directly proportional to the concentration of well-dispersed chains in solution. It is noted that, whereas solution viscosity depends both on polymer concentration and polymer mass, experiments for given polymers all involve the same polymer and hence the same polymer mass distribution, and so the dilute solution viscosity is unambiguously proportional to the concentration of dissolved polymer.

It is important to point out that, while the method of Kravtchenko et al. (1999) used here gives highly reproducible results, even under nondispersing conditions, our early attempts at measuring viscosity vs. time for dissolving powders led to highly erratic results, which resembled a form of constrained chaos. Seemingly slight variations in how the powder was added to the system, how it was stirred, and so forth, led to unique and irregular time courses for dissolution, which, however, would always end at the same final value after complete dissolution. These chaotic paths presumably were due to a wide variation in how lumps were immediately formed upon addition, and how poorly controlled shear rates could occasionally break lumps open, causing transient increases in the slope of viscosity vs. time. The definition of a technique to obtain reproducible dissolution curves, even under nondispersing conditions, was a key factor.

Table 1 lists weight average molecular weights, M_w, peak masses, M_{peak}, and weight average intrinsic viscosity, $[\eta]_w$, for the different polysaccharides used. These results were obtained by size-exclusion chromatography (SEC) with coupled multiangle laser light scattering, refractometer, and viscometer detectors, as previously described (Reed, 1996). Also shown are the values of the dissolution rate constant, k, discussed below. No SEC data are available for the carrageenan series, which was produced by acid hydrolysis. The increasing number from D18 to D63 indicates the viscosity (in mPa·s) of a 1 % solution in distilled water at 70°C.

Table 1. Dissolution Rate Constants k, and Some SEC Characterization Results

	k (μm/s)	M_w	M_{peak}	$[\eta]$ (mL/g)
Pectin A	0.45	86,000	45,000	376
Pectin B	0.96	116,000	63,000	497
Guar	0.067	1,200,000		1,090
Carrageenan, D19*	1.73	XX	XX	367
Carrageenan, D30*	1.90	XX	XX	XX
Carrageenan, D50*	1.90	XX	XX	
Carrageenan, D68*	2.08	XX	XX	570
Xanthan	0.044	5×10^6	XX	XX

*No SEC molecular weight data available. Viscosities indicate mass increases going from D19 to D68.

Qualitative Observation on the Polymeric Grains and Lump Formation

Observations under a microscope showed that the dry grains in this study have a wide variety of structure, including long, fibrous-type strands and bulky, blocklike pieces with well-defined edges but no discernible geometric shape.

To visualize the lump-formation process one gram of sieved material of the largest fraction (200 to 250 μm) and, separately, the smallest (45 to 63) fraction was dumped onto the surface of still water. The fine grains hit the surface and remained in a heap, floating above the water level, still dry. The effects of surface tension could be seen by the water bending away from the horizontal plane around the edges of the slowly hydrating heap. Tens of seconds later the underside of the heap was hydrated into a visible, homogeneous gel layer, from which polymer chains dissolve into solution. The floating pile thus consists of a hull of dissolving gel, surrounding a bed of dry, heaped material.

Dumping the bed of coarse grains onto the surface gave quite a different result. The bed immediately plunged deeper than that of the fine grains. Hydration also began quickly, and visible chunks of gel could be seen falling from the bottom of the shell of the dissolving gel, before this latter finally ''skinned over'' into a uniform hull, as in the case of the fine grains. There was, reproducibly, a much smaller fraction of dry materials atop the floating heap than in the fine-grain case, and the whole pile remained more deeply immersed in the water. Left undisturbed, the dissolution process of the gel is extremely slow, and remains as one large dissolving lump.

A lump, then is a ''sack'' of dry grains encapsulated in a homogeneous skin of gel. Lumps ultimately form because in the process of polymeric swelling and gel formation all the voids between pores are filled up with gel, which is itself only sparingly permeable to water where it is dense. Lump formation takes place within moments of the dry grain bed contacting the solvent. The time for lumps to form is much shorter than the characteristic time for dissolution of individual grains. Hence it can be asserted that lumps form immediately or not at all.

Background Theory

Hydrodynamic regime

Considering the three dissolution steps mentioned earlier, the evidence suggests that Step 2 is the rate-controlling step. It appears that Step 1 occurs rapidly, because there is very little detectable delay between adding the grains and observing the onset of the cubic time-dependent regime characteristic of Step 2. Furthermore, there is no deviation from the cubic time-dependence characteristic of Step 2 at the outset of the experiment, which is actually linear at early times, indicating that the kinetics of gel layer formation is not convoluted with Step 2, so that this is also not a mixed heterogeneous reaction. Step 3 is not rate limiting because the experiments are carried out in the limit of high Peclet number, *Pe*, so that dissolved polymer chains are swept rapidly into the bulk by convection and do not linger as a thickening layer of dispersed, slowly diffusing chains. *Pe* is (mass transfer by convection)/(mass transfer by diffusion), and can be estimated as follows:

$$Pe = UL/D, \tag{1}$$

where U is the characteristic flow velocity of the solvent with respect to a grain, L is the characteristic length scale, which can be taken as the gel layer thickness, and D is the polymer diffusion rate in the bulk. It is assumed that the experiment takes place in a laminar regime of the stirred dissolution bath. If the flow is turbulent, then it is expected that convective transport of chains into the bulk will be even faster, making the case for Step 2 as the rate-limiting step even stronger.

The bath is stirred with a paddle wheel at an angular velocity $\omega = 25$ rad/s, whose vectorial direction is taken as the z-axis. Treating the grain as a sphere of radius R allows the flow to be modeled as follows. A sphere in a shear flow rotates at the same rate as the stirring, so the tangential velocity of the sphere is ωR. Furthermore, this rotation perturbs the flow field around the sphere, causing fluid to flow radially away from the sphere in the second and fourth quadrants, and toward the sphere in the third and fourth quadrants. Here, the origin of the coordinate system is fixed at the particle's center, with the x-axis in the instantaneous direction of flow of the fluid at the particle's center, and the y-axis is hence radially outwards from the center of the stirred bath.

Now, to first order, the x, y, and z components of the fluid velocity with respect to the sphere, u, v, and w, respectively, are given by (Sadron, 1953; Einstein, 1956)

$$u = \frac{-5R^3\omega x^2 y}{2r^5}, \qquad v = \frac{-5R^3\omega xy^2}{2r^5}, \qquad w = \frac{-5R^3\omega xyz}{2r^5}, \tag{2}$$

where r is the radial distance from the center of the sphere ($r \geq R$) to any point in the flow field. At the surface of the grain ($x = y = z = R$), hence, liquid containing released polymer chains can be transported away with a speed of up to

$$u = 2.5\omega R, \tag{3}$$

where R, the hydrated grain radius, typically starts on the order of 10^{-2} cm, and then decreases as dissolution proceeds. Typical diffusion constants for a polymer of equivalent hydrodynamic radius of 50 nm in water at $T = 25$°C are $D = 10^{-7}$ cm^2/s. An extremely conservative estimate of the gel layer thickness is that it is at least on the order of the contour

length of an individual polymer. For the pectins and xanthans used, this should be in the range of 1–10 μm. Conservatively taking $L \sim 1$ μm yields an initial $Pe = 625$. As the grain shrinks, *Pe* will likewise decrease. Note, however, that even in the unrealistic case of a grain having shrunk to the very gel layer thickness of 1 μm, *Pe* is still 6.25.

Another way of viewing the relative rates of convection vs. dissolution is to compare, via Eq. 3, the time it takes a solvent containing polymer to flow an entire grain radius away from the surface. This time is given simply by $1/2.5\omega = 0.016$s, and is independent of grain size. Comparing this to typical dissolution times of hundreds to thousands of seconds (presented below) shows that convection is far faster than dissolution.

Hence, $Pe \gg 1$ throughout the entire grain dissolution process. This means that released polymer is swept into the bulk as quickly as it appears, so that the concentration difference of polymer (and water) between the interior and exterior of the gel layer is probably constant; that is, close to 100% polymer on the interior and close to 0% at the outside of the layer. This case represents a limiting flux of released polymer chains, and this may well be why the simple cubic dependence predicted by the constant flux model presented below fits the data so well; the flux J really is constant throughout dissolution, because we are in the limit of maximum flux throughout.

Dissolution of spherical, monodisperse grains

Consider a spherical grain of initial radius R_0 and density ρ_0. It is placed in a solvent and, after an initial wetting period (Step 1), begins to shed polymer chains into solution, measurable in terms of a mass flux, J, defined as the mass of polymer chains shed per unit surface area per unit time. We assume that J remains constant from time zero, that is, that the wetting period is negligibly short compared to the dissolution time of the grains. Mass, M, is then lost from the grain at a rate:

$$\frac{dM}{dt} = -4\pi JR^2, \tag{4}$$

which, for constant J, gives a solution of the form

$$M(t) = \frac{4\pi\rho_0}{3}(R_0 - kt)^3, \qquad kt \le R_0, \tag{5}$$

where $k = J/\rho_0$ is the volume flux. The concentration of dissolved polymer as a function of time, $C_p(t)$, is then

$$C_p(t) = C_0\left[1-(1-kt/R_0)^3\right], \qquad kt \le R_0, \tag{6}$$

where C_0 is the initial mass concentration of grains in solution. Equation 6 indicates that dissolution is a finite process, not asymptotic. That is, the polymer is totally dissolved at $t = R_0/k$. If $C_p(t)$ is measured experimentally, by viscometry, for example, then the initial slope defines the curve completely, since k/R_0 is the only parameter. The reduced initial velocity v_{in} is then given by

$$V_{\text{in}} \equiv \frac{1}{C_0}\frac{dC_p(t)}{dt}\bigg|_{t=0} = \frac{3k}{R_0}. \tag{7}$$

Any physical quantity proportional to concentration of dissolved material can be used to measure the dissolution kinetics: viscosity, refractive index increment, and so forth.

It is noted in connection with Eq. 7 that what is actually determined is the characteristic dissolution time, which can be related to k and R_0 for an equivalent dry, unhydrated sphere, whose size is known prior to dissolution by sieving or other sizing methods. In reality, the particles' surfaces quickly swell, forming an outer gel layer that immediately begins to dissolve, but there is some microscopic evidence that there remains a dry core that continues to hydrate as dissolution proceeds, so that the equivalent dry radius parameters are still conceptually useful. For the case of lumps, direct recovery and analysis shows that they have dry cores, even though gel formation occurs more rapidly than dissolution, always leaving the latter as the rate-limiting step.

Extension to nonspherical grains

Any three-dimensional body can be described by characteristic length scales x, y, and z, such that the volume V and surface area A are related (via the integration factors appropriate to the actual geometry of the body) as

$$V = axyz \qquad \text{and} \qquad A = bxy + cxz + dyz, \tag{8}$$

where a, b, c, and d are constants. Using the same assumption of a constant surface flux J, $C_p(t)$ is given by

$$\frac{C_p(t)}{C_0} = 1 - \left(1-\frac{dJ}{ax}t\right)\left(1-\frac{cJ}{ay}t\right)\left(1-\frac{bJ}{az}t\right). \tag{9}$$

From this, a cubic time dependence is expected for any object whose three characteristic dimensions are comparable, a squared time dependence for those for which one dimension is considerably larger than the other two (such as a long rod or fiber), and linear for an object for which one dimension is considerably smaller than the other (such as disks or flakes).

Dissolution of polydisperse grains

If polydisperse powder is added to the solvent, then the grains will hydrate and lumps may form to produce an initial hydrated population of grains and lumps $c_o(R)$, where $c_o(R)\,dR$ is the mass concentration of grains or lumps in the interval of radii R to $R + dR$, and is subject to the normalization condition

$$C_0 = \int_0^\infty c_o(R)\,dR. \tag{10}$$

Once $c_o(R)$ is established, the grains then begin to dissolve according to a time-dependent "dissolution transform" $D(R, t)$, which yields $C_p(t)$, for a given initially wetted popu-

lation of grains and lumps, $c_o(R)$:

$$C_p(t) = \int_0^\infty c_o(R)\, D(R,t)\, dR, \tag{11}$$

where the kernel of the transform $D(R,t)$ will depend on the dissolution model. For the constant mass flux model presented earlier, $D(R,t)$ is identical in form to Eq. 9, which for spheres is given by

$$D(R,t) = 1-(1-kt/R)^3 \quad \text{for} \quad kt \le R \tag{12}$$
$$= 0 \quad \text{for} \quad kt > R.$$

Substituting Eq. 12 into Eq. 11 gives

$$C_p(t) = \int_0^\infty c_o(R)\left[\frac{(kt)^3}{R^3} - 3\frac{(kt)^2}{R^2} + 3\frac{kt}{R}\right] dR, \tag{13}$$

subject to the condition on the integrand, that the integrand equals zero for $kt/R \ge 1$.

Taking the initial slope of $C_p(t)$ yields, according to the definition of V_{in} in Eq. 7,

$$V_{\text{in}} = \frac{3k}{R_{S,0}}, \tag{14}$$

where $R_{S,0}$ is the initial surface-averaged radius of the entire polydisperse population of wetted grains and lumps, which, by definition is

$$R_{S,0} = \frac{\int_0^\infty R^3 N(R)\, dR}{\int_0^\infty R^2 N(R)\, dR}, \tag{15}$$

where $N(R)$ is the number density of particles. This becomes, for spheres where $c_o(R) \alpha R^3 N(R)$,

$$R_{S,0} = \frac{C_0}{\int \frac{c_o(R)\, dR}{R}}. \tag{16}$$

Bimodal Approximation

Now, the long-term behavior of a polydisperse dissolution problem must be approached carefully because of the condition that $kt/R < 1$ on the integrand of Eq. 13. Say that after the initial coalescence into lumps, the polymer in solution is present as a certain concentration of unlumped grains $C_{g,0}$, and the rest is in the form of lumps $C_{l,0}$, such that $C_0 = C_{g,0} + C_{l,0}$, and one has a bimodal population, each with its own width and polydispersity, but fairly well separated, that is, that lumps are much larger than grains. There is considerable experimental justification for this, since inspection of lump-forming solutions showed the lumps to be on the order of millimeters, whereas the grains are on the order of tens or hundreds of microns. $C_p(t)$ can then be represented as

$$C_p(t) = \int_0^\infty c_{g,o}(R)\left[\frac{(kt)^3}{R^3} - 3\frac{(kt)^2}{R^2} + 3\frac{kt}{R}\right] dR$$
$$+ \int_0^\infty c_{l,0}(R)\left[\frac{(kt)^3}{R^3} - 3\frac{(kt)^2}{R^2} + 3\frac{kt}{R}\right] dR, \tag{17}$$

where the integrands are again zero for $kt \ge R$, and the initial grain and lump distributions, $c_{g,o}(R)$ and $c_{l,o}(R)$, respectively, obey the normalization conditions

$$C_{g,0} = \int_0^\infty c_{g,0}(R)\, dR \quad \text{and} \quad C_{l,0} = \int_0^\infty c_{l,o}(R)\, dR. \tag{18}$$

Thus, the initial velocity is

$$V_{\text{in}} = \frac{3kf_g}{R_{S,g,0}} + \frac{3k(1-f_g)}{R_{S,l,0}}, \tag{19}$$

where the same type of equivalent dry grain notion is used for k and $R_{S,l,0}$ for the lump population. Here $R_{S,g,0}$ is the initial surface average radius of dispersed grains, and $R_{S,l,0}$ is the initial surface average radius of the lumps. Here f_g is the mass fraction of material in the form of grains (and small lumps, rather than large lumps), that is

$$f_g = C_{0,g}/(C_{0,g} + C_{0,l}). \tag{20}$$

If $R_{S,l,0} \gg R_{S,g,0}$, then at $t = R_{S,g,0}/k$ one is still in the initial regime of the second term in Eq. 17, so that

$$C_p(t) \cong C_{g,0} + \frac{3ktC_{l,0}}{R_{S,l,0}}. \tag{21}$$

In terms of the dimensionless concentration formulation:

$$\frac{C_p(t)}{C_0} = f_g + \frac{3kt(1-f_g)}{R_{S,l,0}}. \tag{22}$$

Thus, in this long time regime, drawing in the best tangent to the dimensionless concentration data gives the fraction of material remaining as grains, f_g, from the intercept with the origin, and the slope gives the long term velocity V_{long}:

$$V_{\text{long}} \equiv \left.\frac{dC_p(t)}{C_o dt}\right|_{t \gg R_{N,g,0}/k} = \frac{3k(1-f_g)}{R_{S,l,0}}. \tag{23}$$

The dissolution process of a bimodal distribution of particles under nondispersing conditions can be analyzed with two fitting parameters, V_{in} and V_{long}, obtained from linear fits to initial and final slopes. From these, there are four parame-

ters that characterize the process: $R_{S,g,0}$, $R_{S,l,0}$, f_g, and k. The first three are immediately obtainable from the two fit parameters, since the y-intercept determined uniquely from V_{long} directly yields f_g, whereas k is best obtained by at least one dissolution experiment of a sieved fraction of known average radius under dispersing conditions. The flux J is computed by $J = \rho_o k$, where ρ_o is the initial density of a grain. Inspection of Eqs. 14 and 19 yields a reciprocal addition rule for the surface averages:

$$\frac{1}{R_{S,0}} = \frac{f_g}{R_{S,g,0}} + \frac{(1-f_g)}{R_{S,l,0}}. \tag{24}$$

Application of the bimodal approximation allows the surface averages of the subpopulations of grains/small lumps and large lumps to be estimated, instead of finding only the composite surface average $R_{S,0}$, which is obtained when no assumptions on the form of the polydispersity are made.

The bimodal approximation is valid for any distribution, since, due to the fact that the integrand goes to zero for $kt \geq R$, any distribution can be defined as ''bimodal'' in the following operational way: The first ''mode'' (small R), whose $R_{S,g,0}$ is computed via Eq. 14 is actually the surface average of all particles whose initial radius is smaller than the radius of particles that have completely dissolved at the time t from which the start of the tangent to the long-term slope is determined. Similarly, the second mode (large R), whose $R_{S,l,0}$ is computed by Eq. 21, is actually the surface average over all remaining, undissolved particles commencing at this same time t from which the start of the tangent to the long-term slope is determined.

Results and Discussion

Figure 1 shows examples of typical dissolution curves for pectin A, under dispersing and nondispersing conditions, respectively. Also shown in the figure are the curves obtained from using the limiting slopes and intercepts in the preceding equations. Table 2 summarizes the experimental conditions and the fitting parameters for each curve. Under dispersing conditions, the fit is to the single parameter, V_{in}, found simply from the initial slope of the dissolution curve.

The fit for unsieved pectin under nondispersing conditions is made using the bimodal treatment for a polydisperse system of grains and lumps given earlier, and requires two parameters, V_{in} and V_{long}, found from the initial and final tangents to the curve according to Eqs. 14 and 23. The two kinetic parameters, $k/R_{S,g,0}$ and $k/R_{S,l,0}$, in Table 2 are found from V_{in} and V_{long} by

$$\frac{k}{R_{S,g,0}} = \frac{V_{\text{in}} - V_{\text{long}}}{3f_g} \tag{25}$$

and

$$\frac{k}{R_{S,l,0}} = \frac{V_{\text{long}}}{3(1-f_g)}. \tag{26}$$

The fraction of grains f_g is found from the y-intercept of the final tangent line. These parameters can then be substituted into

$$C(t) = \text{Base} + \left(C(t_f) - \text{Base}\right)\left\{ f_g\left[1-\left(1-\frac{kt}{R_{S,g,0}}\right)^3\right] + (1-f_g)\left[1-\left(1-\frac{kt}{R_{S,l,0}}\right)^3\right]\right\} \tag{27}$$

to plot the resulting fit curve shown in Figure 1. Here $C(t)$ refers to relative concentration in arbitrary units, and Base is the pure solvent-level base line.

The agreement of the model with the nondispersing data in Figure 1 suggests that (1) the hydrated grains really can be treated as a bimodal population of small grains/small lumps and large lumps; (2) these latter dissolve at a constant flux J,

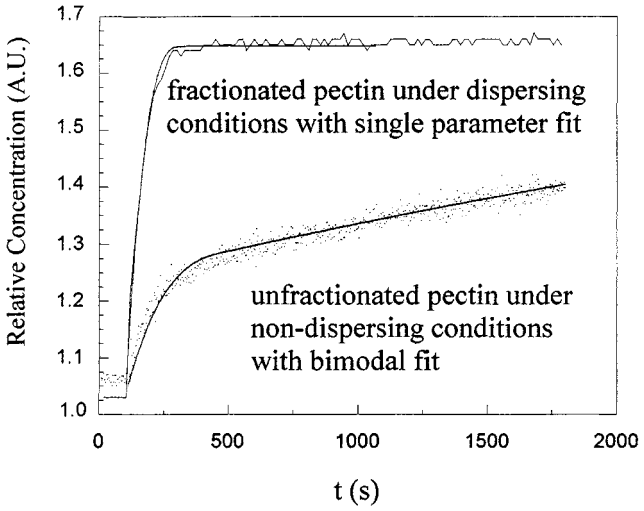

Figure 1. Typical dissolution curves for sieved pectin (125–212 μm) under dispersing conditions and for unsieved pectin under nondispersing conditions.

Under dispersing conditions a linear fit to the initial slope gives V_{in}, which yields the well-matched curve shown, using Eq. 6. For the unsieved data under nondispersing conditions, where lump formation is extensive, V_{in} and V_{long} were taken from the initial and long-term slopes, respectively, and the resulting curves, computed according to Eq. 27 gives a good match to the data.

Table 2. Pectin A Parameters for the Computed Curves of Figure 1

Sample	125 μm Pectin (w/Dispersant)	Unsieved Pectin (No Dispersant)
Base	1.03	1.10
$C(t_f)$	1.65	1.68
C_{int}	1.65	1.28
$C(t_f)$-base	0.62	0.58
f_g	1.0	0.31
V_{in} (fit parameter)	0.0140	0.0026
V_{long} (fit parameter)	X	1.72×10^{-4}
$k/R_{S,g,0}$	0.0047	0.00262
$k/R_{S,l,0}$	X	8.31×10^{-5}

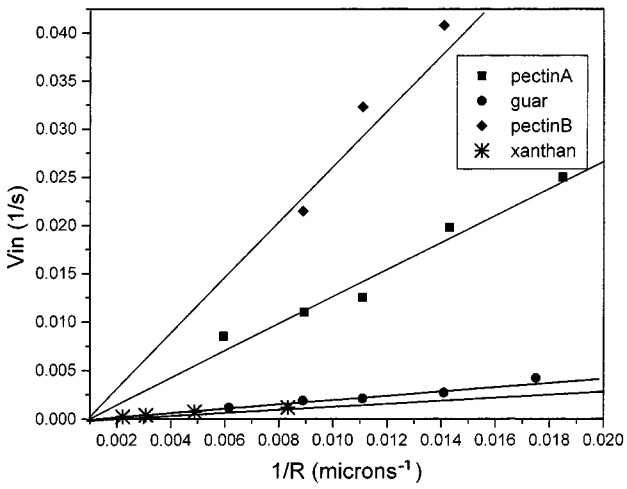

Figure 2. V_{in} vs. $1/R$ for guar, pectins A and B, and xanthan under dispersing conditions.

The slope yields the dissolution rate constants k in Table 1.

so that both the grains and lumps dissolve in the constant, limiting flux case of high Peclet number; (3) the dissolution of the lumps, no matter how irregular they might be, conforms well to dissolution of an equivalent bulky, three-dimensional (3-D) object; and (4) the bimodal approach is a robust procedure. While there is no direct evidence that the constant dissolution flux J of the large lumps is the same as for grains, the fact that it is constant suggests that it might be equal or similar to the one of the daughter grain particles of which they are composed. This allows values for lump size to be computed that agree with direct observations.

Dissolution rate is inversely proportional to grain size for pectin and xanthan

Equation 14 predicts that the initial dissolution velocity of a grain V_{in} is inversely proportional to its initial wetted radius. Figure 2 shows V_{in} vs. $1/R$ for two different pectin lots, a xanthan sample, and a guar sample. The linearity of V_{in} vs. $1/R$ in Figure 2 further confirms the usefulness of the constant mass flux model and shows that, even though the grains are not spherical, they can be treated as equivalent spheres in terms of their surface area, which scales as the square of the average sieved diameter. The slope of the data in Figure 2 yields k via Eq. 14. Table 1 gives the resulting values of k for the different samples. The value of the flux J can be found from k by $J = k\rho_o$, where ρ_o is the density of a dry grain, which is close to 1.75 g/cm^3 for all the polysaccharides used.

It is seen in Figure 2, as well as Table 2, that the initial dissolution rates, V_{in}, of guar and xanthan are over ten times slower than those for pectin and carrageenan of similar initial grain size. In fact, k for carrageenan is 50 times greater than for the xanthan. This may be related to the fact that pectin and carrageenan both have lower molecular weight and are more flexible (lower persistence length) than xanthan.

Although the carrageenan molecular mass was not measured directly, the relative solution viscosities indicated that the mass was measurably higher for the largest fraction compared to the lowest mass fraction, yet the value of k in Table 1 shows no noticeable dependence on the mass. Further, systematic work is needed to define the effects of molecular mass and persistence length.

Initial dissolution rates V_{in} with no dispersant are surprisingly similar for all grain sizes

Analysis of V_{in} shows that when no dispersant is used, V_{in} is independent of the grain size. For example, the average of 15 curves for pectin A gave $V_{in,ave} = 0.00447(s^{-1}) \pm 15\%$. This is a remarkably narrow distribution for V_{in}, considering that V_{in} for sieved fractions with dispersant varies systematically by a total factor of 100% in going from the smallest to largest grains. Figure 3 shows V_{in} and V_{long} for two pectin samples and guar.

An empirical, and rather speculative explanation for this, is that $V_{in} \gg V_{long}$, as Figure 3 shows, so

$$V_{in} \cong \frac{3kf_g}{R_{S,g,0}}. \tag{28}$$

Since the fraction of material remaining as grains (or small lumps), f_g, decreases as $R_{S,g,0}$ decreases, the two effects should counteract each other. It is nonetheless remarkable that they balance so closely as to keep V_{in} fairly constant.

Finally, it should be pointed out that, the surface average radius $R_{S,0}$, of the *entire* population of grains and lumps is given by Eq. 14, so that a constant V_{in} leads to the remarkable conclusion that $R_{g,0}$ is constant and independent of the initial grain size. For the sieved fractions, using the average value of $V_{in} = 0.00447$, yields $R_{S,0} = 300$ μm.

Lump radii $R_{S,l}$ are on the order of millimeters for all initial grains sizes

Determination of V_{long} is less precise than for V_{in} because the long-term slopes are shallower than in the V_{in} case, and hence the signal-to-noise ratio is lower. The ensuing $R_{S,l,0}$ are not very precise, but the lumps associated with these data

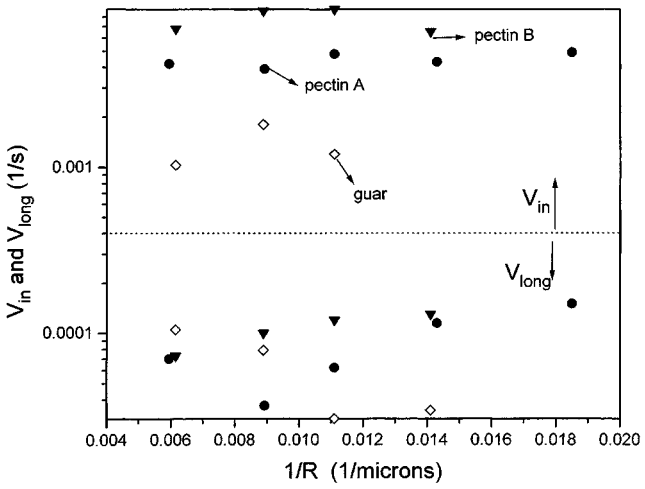

Figure 3. V_{in} and V_{long} under nondispersing conditions for pectins A and B and guar.

are typically several millimeters in radius. Visual observation shows that this figure is of the right order of magnitude. It is hard to discern a trend for $R_{S,l,0}$ vs. initial grain size, and it may be stated approximately that when lumps form, their size is essentially independent of the initial grain size $R_{S,g,0}$, whereas the fraction of material in lumps decreases inversely with $R_{S,g,0}$.

Mass fraction in lumps decreases with increasing grain radius

The mass fraction of grains, f_g, was computed from the intercept of the slope of the long dissolution component at $t = 0$. The data of fraction of lumps $(1 - f_g)$ for two different pectin lots, and for guar, is shown in Figure 4. For all three data sets there is a nonzero x-intercept. The nonzero intercept is a cutoff radius, such that for initial grain radii larger than or equal to R_c, no lump formation at all occurs. For pectin A and guar studied under the constant solvent and shear conditions of this work, initial grains of $R_{S,0} = 340$ μm do not form lumps. The pectin B value is $R_{S,0} = 250$ μm.

The potential significance of this finding should not be overlooked. Since lumps sizes are on the order of a millimeter, or 30 times larger than the 340-μm optimum grain size of the pectin lot studied here, it would take 30 times longer for complete dissolution of a solution containing lumps. For this lot, *complete* dissolution with lumps takes several hours. The practical point is that grinding polymer powders more and more finely to reduce the dissolution time eventually becomes counterproductive because it leads to increased lump formation.

It is expected that a number of factors should determine the optimum cutoff radius. The motion of the solvent surface under stirring should be important in producing a shearing force that can separate the initial powder bed into separate lumps. The surface motion may also give some layering of grains falling on the surface. The limit of static solvent can give extremely high lump formation. For example, when the quantity of powder used in the present experiments is dumped onto a stationary solvent surface, the whole powder bed becomes a single large lump whatever the grain size. The initial packing of the powder bed should also have a substantial influence on lump formation, in that the more densely it is packed the higher the tendency for lump formation should be.

Dissolution of polydisperse grains under dispersing conditions is simply the sum of the individual components of the dry size distribution

Figure 5 shows data for both sieved and unsieved guar under dispersing conditions. The dissolution behavior for the unsieved fractions falls mainly between the data for the large and small sieved fractions. However, the initial slope is actually higher than for the small sieved fraction. This is quite reasonable, since the unsieved lots contained grains even smaller than the smallest sieved size, as the grains that passed through the smallest sieve were discarded. The behavior of the unsieved sample is exactly what is expected for the case in which no lumps form, and confirms the validity of Eqs. 11 and 12; that is, linear superposition, as expressed by the integral transform.

Dissolution of polydisperse grains under nondispersing conditions is not simply the sum of the individual components of the dry size distribution

Figure 6 shows data for sieved and unsieved guar under nondispersing conditions. The striking aspect of this result is that the formation of lumps for the unsieved fractions does not fall between the curves for the sieved lots, and is as bad or worse than that of the smallest grain size in the sieved lots.

This behavior implies that the dissolution of a polydisperse power under nondispersing conditions cannot be treated as

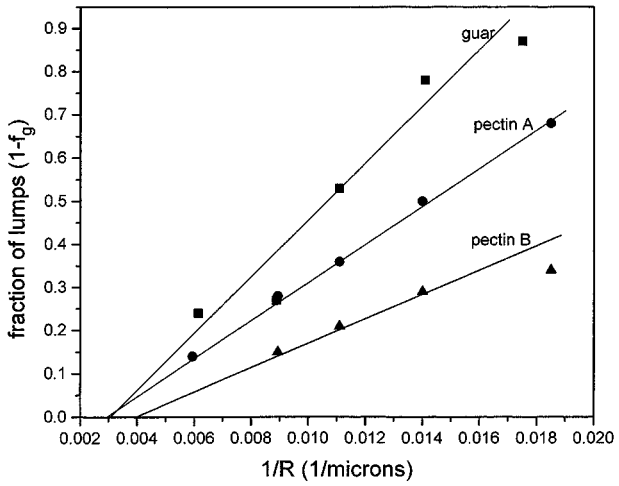

Figure 4. The fraction of material in lumps $(1\text{-}f_g)$ vs. $1/R$ for guar and pectins A and B.

The value of $1/R$ at which there is no lump formation (x-intercept) is remarkably similar for the samples.

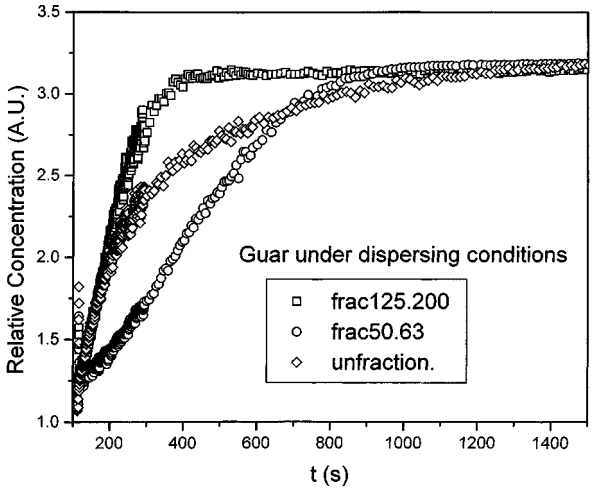

Figure 5. Sieved and unsieved data for guar under dispersing conditions.

The unsieved data falls between the data for the small and large fractions, and is a linear superposition of individually dissolving grains, as expressed in Eq. 11.

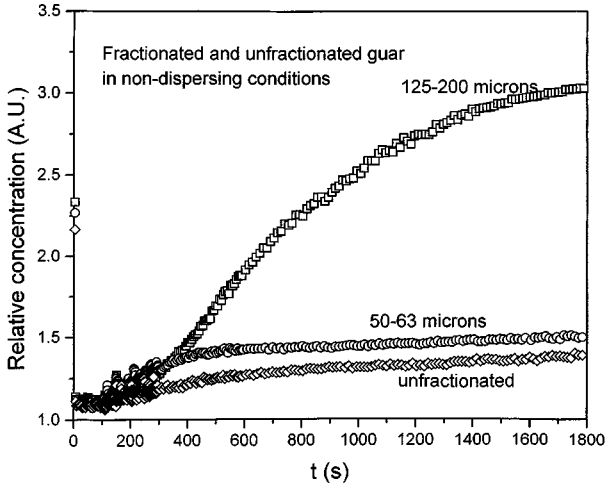

Figure 6. Sieved and unsieved data for guar under nondispersing conditions.

The unsieved data are not a superposition of the extreme size fractions, indicating the formation of lumps. A coalescence transform is suggested for this process in Eq. 29.

an integral transform of the unhydrated particle-size distribution with $D(R,t)$, as earlier. Rather, there should exist a coalescence transform for given solution agitation, and so on, that changes the initial unhydrated, unlumped particle-size distribution $c_d(R)$ into an initial distribution of grains and lumps,

$$c_o(R) = \int_0^\infty c_d(R'_d) F(R'_d, R)\, dR'_d, \tag{29}$$

where $F(R'_d, R)$ is the kernel of the transform, which contains all the physics of how particles of unhydrated initial size R'_d turn into a population of wetted particles with a given distribution. Then $c_o(R)$ dissolves according to the integral using $D(R,t)$ as the kernel. A fundamental study of lump formation would center on developing a theoretical model for $F(R'_d, R)$. In light of our microscopic observations concerning the irregularity of the grain shapes for pectins, guar, and so forth, a useful model with predictive power could not be realistically based on the notion of a collection of polydisperse spheres.

Some remarks on a theory of lump formation

Lump formation is not an equilibrium process. Either the lumps form immediately or they do not form at all. Thus, adding a powder slowly to the solvent avoids lump formation, as the grains hydrate separately, whereas if all the powder is added at once, the grains can stick together.

Lump formation is due to the relative importance of two processes. First, grain separation due to collapse of the porous powder bed under its own weight or agitation, and second, the grains swelling to form a sticky, low permeability layer at the outside of the lump. Grains will disperse if separation dominates, whereas lump formation will occur if swelling blocks the pores between the grains before they can separate to dissolve separately.

The pore-blocking notion can be formulated as follows. Let J_w be the solvent influx rate into a grain (g/cm^2·s), taken as constant to a first approximation. Solvent influx occurs for a short period, t_e, until a gel layer of thickness T_g is formed. After this, dissolution of the grain takes place according to the model already described. It is before t_e that any lumps form. *A priori* we don't know t_e, but, based on qualitative observations, it is probably on the order of a few seconds.

Expressing the swelling of a spherical grain in terms of mass increase due to influx of solvent gives

$$\frac{dR}{dt} = \frac{J_w}{\rho_w}, \tag{30}$$

where ρ_w is the density of the solvent. For constant J_w the radius of the particle hence grows as

$$R(t) = R_0 + \frac{J_w}{\rho_w} t. \tag{31}$$

The pores between grains in a randomly packed powder bed are defined by the volume of the space between grains. Elementary considerations require that the average effective "pore" radius, P, between spheres scale linearly with sphere radius R. Hence, the critical time for pore blockage t_b is proportional to R, via

$$t_b \propto \frac{\rho_w}{J_w} R_0. \tag{32}$$

Since t_b increases linearly with R, then, all else being equal, it is expected that pore blocking decreases with increasing particle size. This trend is indeed observed. In practice t_b must be compared to a characteristic dispersing time t_d in order to form a blocking condition (such as via a dimensionless parameter). Since we currently do not have a model for t_d, we can't precisely define the limit for pore blocking.

It is assumed that capillary flow effects and surface tension effects, while possibly present, are secondary to the pore-blocking effect in determining lump formation. We have some evidence for this, as reducing the surface tension by adding surfactant to the water before powder addition did not significantly change the results. However, we noticed a remarkable effect on the dispersibility when a small amount of solid surfactant is mixed with the powder before addition: when the powder bed hits the water, the grains "explode" in all directions and lump formation is eliminated. We attribute this to the Marangoni effect, that is, surface flow up the surface tension gradient (see, for instance, Probstein, 1994). This observation can be a useful way to improve powder dispersibility in industrial practice.

To have a macroscopic theory of lump formation requires a relationship between the pore-size distribution and the fraction of lumps. We envisage a percolation theory approach where the fraction of powder in lumps is related to the fraction of blocked pores (bonds). Determination of how the pore-size distribution depends on the particle-size distribution and packing density for irregular-shaped particles is daunting. The simpler problem of packing of polydisperse

spheres has been treated extensively (Ouchiyama and Tanaka, 1984).

Summary and Conclusions

The important kinetic parameters governing polymer powder dissolution and useful size averages from polydisperse populations of grains and lumps have been defined for a model in the limit of high Peclet number. A simple technique for analyzing data for polymer concentration during dissolution is developed using two linear fitting parameters. These parameters allow characterization of the dissolution process in terms of the fraction of material in grain/small lump form, f_g, the initial and long-term dissolution rates, V_{in} and V_{long}, respectively, and the kinetic constant, k (from which the mass flux for dissolution, J, can be computed). With no assumptions about the type of distribution, the initial surface average radius of the entire grain/lump population $R_{N,0}$ can be computed from these parameters. Under a bimodal approximation, which is shown to actually hold operationally for more general distributions, the surface averages of the grain/small lump population and the lump population can be computed, and are denoted, respectively, as $R_{S,g,0}$ and $R_{S,l,0}$. The lump formation process itself is extremely complicated, but the governing notion is that competition between the time it takes to disperse the grains under stirring and the time it takes to block the pores between the grains due to the grains swelling with solvent determines the extent of lump formation.

Conclusions concerning lump formation include the following: (1) for given dissolution conditions and a specific lot of polymer, an ideal grain size exists, larger than or equal to which no lumps form. This grain size appears roughly equal to the surface average size of the entire, initially hydrated grain/lump population $R_{N,0}$. (2) The smaller the grains, the greater the mass fraction in lumps. (3) Since lump formation increases with decreasing grain size, it is counterproductive to mill dried polymers into very fine grains. (4) It is probably best to disperse grains into solution initially with as much free volume per grain as possible; such as by ''blowing'' them into solution, or introducing them as a stream of particles.

As noted in this work, the constant k (or J) and the tendency of grains to form lumps are the two most important parameters governing the speed of dissolution. It is expected that k is largely controlled by polymer molecular weight and architecture, solvent conditions, and the thermodynamic processes such as precipitation and drying by which the dry grains were formed. The data here indicate that the tendency to form lumps is largely governed by the grain size, although the constitution of the grain due to dry grain production thermodynamics as well as solvent conditions are also expected to be relevant.

We conclude that there is an optimum powder grain size (distribution) for avoiding lump formation. If the grains are too small, lumps will form. If they are too large, dissolution will be too slow. However, it is clear that the optimum is not universal. If the powder is dissolved using violent mixing, the optimum grain size will be lower, as lumps that would be a problem with gentle mixing are broken up. Experience shows that it is best to err on the side of grains that are too large, as the increase in dissolution time in this case is small, whereas the dissolution time of lumps is typically at least an order of magnitude larger than that of even very large grains.

Coupling Kravtchenko's experimental method with the data analysis described here provides a powerful method for the detailed study of other effects not addressed here, such as electrostatic charge, ionic strength, and temperature, on powder dispersibility.

Acknowledgments

One of the authors (W.R.) acknowledges support from LA BoR grant RD-B-11.

Literature Cited

Buckley, D. J., and M. Berger, ''The Swelling of Polymer Systems in Solvents. II. Mathematics of Diffusion,'' *J. Poly. Sci.*, **56**, 175 (1962).

Brochard, F., and P. G. de Gennes, ''Kinematics of Polymer Dissolution,'' *Physicochem. Hydrodynam.*, **4**, 313 (1983).

Devotta, I., V. Premnath, M. W. Badiger, P. R. Rajamohanan, S. Ganapathy, and R. A. Mashelkar, ''On the Dynamics of Mobilization in Swelling-Dissolving Polymeric Systems,'' *Macromol.*, **27**, 532 (1994a).

Devotta, I., V. D. Ambeskar, A. B. Mandhare, and R. A. Mashelkar, ''The Lifetime of a Dissolving Polymeric Particle,'' *Chem. Eng. Sci.*, **49**, 645 (1994b).

Einstein, A., *Investigations on the Theory of Brownian Movement*, R. Furth, ed., Dover, NY (1956).

Herman, M. F., and S. F. Edwards, ''A Reptation Model for Polymer Dissolution,'' *Macromolecules*, **23**, 3662 (1990).

Kravtchenko, T. P., J. Renoir, A. Parker, and G. Brigand, ''A Novel Method for Determining the Dissolution Kinetics of Hydrocolloid Powders,'' *Food Hydrocolloids*, **13**, 219 (1999).

Michel, R. C., and W. F. Reed, ''New Evidence of the Non-Equilibrium Nature of the 'Slow Modes' of Diffusion in Polyelectrolyte Solutions,'' *Biopolymers*, **53**, 19 (2000).

Ouchiyama, N., and T. Tanaka, ''Porosity Estimation for Random Packings of Spherical Particles,'' *Ind. Eng. Chem. Fundam.*, **23**, 490 (1984).

Peppas, N. A., J. C. Wu, and E. D. von Meerwall, ''Mathematical Modeling and Experimental Characterization of Polymer Dissolution,'' *Macromol.*, **27**, 5626 (1994).

Probstein, R. F., *Physicochemical Hydrodynamics*, 2nd ed., Wiley-Interscience, New York (1994).

Ranade, V. V., and R. A. Mashelkar, ''Convective Diffusion from a Dissolving Polymeric Particle,'' *AIChE J.*, **41**, 666 (1995).

Reed, W. F., ''Coupled Multiangle Light Scattering and Viscosimetric Detectors for Size Exclusion Chromatography with Application to Polyelectrolyte Characterization,'' *Strategies in Size Exclusion Chromatography*, P. Dubin and M. Potschka, eds., American Chemical Society, Washington, DC (1996).

Sadron, C., *Flow Properties of Disperse Systems*, J. J. Hermans, ed., North-Holland, Amsterdam, 1953.

Tu, Y. O., and A. C. Ouano, ''Model for the Kinematics of Polymer Dissolution,'' *IBM J. Res. Dev.*, **21**, 131 (1977).

Manuscript received Aug. 27, 1999, and revision received Feb. 22, 2000.